High Sensitivity Surface-Enhanced Raman Scattering in Solution Using Engineered Silver Nanosphere Dimers

Desiré D. Whitmore,[†] Patrick Z. El-Khoury,[†] Laura Fabris,[‡] Ping Chu,[§] Guillermo C. Bazan,[∥] Eric O. Potma,[†] and V. A. Apkarian*,[†]

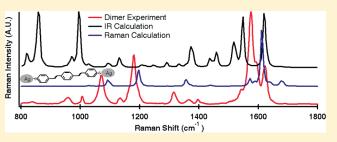[†]Department of Chemistry, University of California, Irvine, Irvine, California 92697, United States

[‡]Department of Materials Science and Engineering, Institute for Advanced Materials Devices and Nanotechnology, Rutgers, The State University of New Jersey, Piscataway, New Jersey 08854, United States

[§]Department of Physics, University of California, Irvine, Irvine, California 92697, United States

[∥]Department of Chemistry, University of California at Santa Barbara, Santa Barbara, California 93103, United States

ABSTRACT: We describe Raman spectroscopy measurements of distyrylbenzene (DSB) molecules equipped with plasmonic antennae in the form of silver dumbbells in aqueous solution under ambient conditions. A synthetic strategy in which the dithiolated molecule is used as the linker between silver nanospheres ensures that the molecules are attached at the intersphere gap where local fields are maximally enhanced. The measured and calculated enhancement factors are in excellent agreement. The reported method has sufficient sensitivity to

also allow for the detection of molecules tethered to single spheres, with 100−1000-fold weaker enhancement. Spectral analysis allows assignment of structures and reveals that in addition to the normal Raman active modes IR active transitions appear in the Raman spectra where field gradients dominate.

■ INTRODUCTION

The enhanced electric fields associated with plasmon excitations at metallic surfaces enable detection of otherwise weak optical signatures of molecules tethered to them. This effect is most evident in surface-enhanced Raman scattering (SERS),[1−4] where the strongly enhanced local fields are exploited to raise the Raman scattered light from a few or single molecules to detectable levels. The ability to probe the Raman response from molecules at such extremely low concentrations not only offers exciting opportunities for molecular sensing[5−7] but also brings fundamental nonfluorescent spectroscopic investigations of single molecules into focus.[8−13]

The feasibility of single-molecule SERS experiments is directly correlated to the magnitude of the field enhancement at a metallic surface. Control over the plasmonic properties of metallic substrates is, therefore, one of the most important parameters in SERS substrate synthesis. Using the strong plasmonic resonances in noble metals, a wide range of SERS substrates have been developed, including electrodes,[2,14] thin films,[15,16] colloidal nanoparticles,[17,18] nanowires,[19,20] and lithographic nanostructures.[21,22] Theoretical calculations have shown that very large local fields are attained in the nanogap of two proximal metallic nanostructures, producing a so-called hot spot in the interstitial region between the structures,[10,23−25] as well as between nanostructure and substrate.[26] A variety of such dimer plasmonic systems have been examined, and field enhancement factors in the nanogap as large as 10^5 have been predicted.[10,24,25] Many SERS investigations over the past decade have been

concerned with the synthesis of systems that take advantage of these hot spots.[27−30] Recent experimental studies have shown that dimeric silver nanospheroids exhibit reproducible high-field enhancement factors. Combined with the chemical enhancement of binding of the chromophore to the substrate, surface-enhanced resonant Raman scattering (SERRS) factors as high as 10^{14} have been reported.[31]

Nanosphere dimers are important model systems that connect theoretical calculations to reproducible experiments and thus form a testbed for quantitative single-molecule Raman experiments. Experimentally, dimer systems are typically formed through spontaneous aggregation upon drying of a colloidal solution.[29] This form of preparation generally produces low yields of dimers and a wide distribution of interparticle separations and orientations. A method which optimizes the colloidal stability has recently been shown to significantly improve dimer formation, producing high yields of dimers with a near-constant nanogap width.[32] Improvements in dimer synthesis are ultimately meaningful only when combined with controlled tethering of molecular targets in the gap. Incorporation of molecules in hot spots is commonly accomplished by drop casting dilute solutions of the target compound onto immobilized substrates. This approach offers limited control of molecular orientation and positioning in the nanogaps. The low yield of successful

metal—molecule—metal systems and the wide distribution of molecular orientations in hot spots have hampered the quantitative capabilities of most SERS assays.

In the present work, we seek to overcome such limitations by employing a synthesis approach of silver nanosphere dimers that directly incorporates the molecular target. Instead of adding the molecular compound after formation of the dimers, we promote dimer formation by virtue of a single molecular linker. Dithiolated conjugate molecules of distyrylbenzene (DSB) are used to form dimers of silver nanospheres in an aqueous solution, which results in a high yield of metal—molecule—metal complexes.[33,34] Because the molecule is held in a fixed orientation in the nanogap, this approach facilitates reproducible SERS measurements. We show that this system allows for SERS measurements in solution with single-molecule sensitivity.

As would be expected from any synthetic approach, the sample contains structural variations. The spectra differentiate between three different types of species: dimers, clusters, and monomers. The SERS spectrum of the dimer resembles that of the bare molecule, whereas unexpected peaks are observed in the monomer spectra. The experimental spectra are assigned based on Density Functional Theory (DFT) vibrational frequency calculations. We find that infrared-active, Raman-forbidden normal modes of DSB appear in the SERS spectra. The change in selection rules can be rationalized to arise from gradients in the local field of the metallic antennae, namely, the gradient field Raman effect.[35] This phenomenon also provides a rationale for fluctuations in the Raman spectrum of an individual structure, to arise from variations in the orientation of the molecule relative to the local field gradients of the plasmon.

MATERIALS AND METHODS

Suspensions of 30 nm Ag nanospheres with a narrow size distribution were prepared following the standard preparation methods for citrate-protected aqueous colloidal solutions.[36,37] Bis(p-sulfonatophenyl)phenylphosphine (BSPP) was added to the citrate-capped Ag nanoparticles to a final concentration of 1 mM. BSPP has a higher affinity for the metal than citrate and provides improved stability of the colloidal solution.[38] We found that relative to citrate the use of BSPP is much preferred for suppressing coalescence and precipitation of the Ag particles. One hour after the addition of BSSP, the dithiolated distyrylbenzene derivative was added. Due to the presence of acetyl protective groups at the thiolated moieties, together with use of BSPP, the reaction was completed within 3 h. For a standard preparation of the Ag colloidal solution, 1 μM of DSB derivative produced the highest yield of dimers in the sample. Purification was achieved via centrifugation in 25% agarose following a speed gradient and yielded solutions with relative amounts of dimers close to 50%.

Sample Characterization. A JEOL-JEM transmission electron microscope (TEM) was used to verify the formation of Ag dimers using an 80 kV acceleration voltage and 200 000× magnification (for an enlarged view of the dimer). The samples were prepared on 200 mesh holey Formvar, carbon-coated copper grids by depositing a drop of nanoparticle solution on the grid for one hour in a controlled humidity chamber to avoid evaporation that could induce some unwanted nanoparticle aggregation.

Scanning electron microscopy (SEM) measurements were performed to determine the concentration of dimers, monomers, and nanoclusters. Droplets (0.1 μL) of the solution were placed
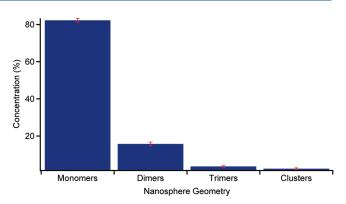

Figure 1. Statistics with standard deviation for the SEM images used to quantify the concentration of dimers in solution after sample degradation, analyzed ∼ 1 year after initial synthesis.

onto clean, aluminum SEM stubs and allowed to dry. After drying, a Zeiss Ultra Plus 55 SEM was used with a voltage of 2 kV to obtain images of each stub. These images include both the entire droplet area (412×), as well as many higher-resolution images (50 000×) taken randomly throughout the droplet area. Within each high-resolution image, the number of single spheres, dimers, and clusters (three or more nanospheres) was counted. Taking the average number of particles per area and then extrapolating to the entire droplet area gives an estimate of the total number of particles for the 0.1 μL volume. Statistics were accumulated from a total of 320 SEM images, with the results shown in Figure 1. The concentration of DSB-linked dumbbells is determined to be no greater than 14.3 pM.

Absorption spectra in the visible range were acquired to characterize the electronic properties of the surface plasmon resonances. The absorption spectra were measured on a Varian Cary 50 UV/vis spectrophotometer using a 10 mm glass cuvette containing the dimer solution.

Raman Microspectroscopy. All Raman data were collected on a microspectrometer consisting of an Olympus IX71 microscope and an Andor Shamrock spectrograph equipped with an Andor iDus cooled CCD. The excitation source was a frequency-doubled Nd:YVO4 laser (Coherent Verdi V5) operating at 532 nm, delivering about 4 mW at the sample position. A water immersion microscope objective (X40, NA 1.15) was used for focusing the excitation light onto the sample. Scattered light is collected in the epi-direction using the same objective, filtered through a holographic notch filter, and steered into the spectrometer. The excitation volume is estimated by integrating the square of the Gaussian beam spot size over the thickness of the slide, i.e. $V_s = \pi \int [w_0(1 + (z/z_R))^{1/2}]^2 dz$, where w_0 is the beam radius at the waist (determined as 0.24 μm) and z_R is the Rayleigh length.[39] To minimize the slide thickness, the sample slide was prepared by sandwiching two glass coverslips together and allowing capillary forces to draw the solution in. The thickness of the slides was determined from optically sectioned coherent anti-Stokes Raman Scattering (CARS) images, recorded on the same microscope setup (for details of the CARS microscope, see ref 40). By tuning the CARS wavelength to the off-resonance frequency dip in the CARS spectrum of water (3600 cm^{-1}), the water signal intensity is minimized, while the glass exhibits a strong nonresonant background, allowing an accurate determination of the location of the glass—water boundary. This method revealed a sample thickness of ∼10 μm. The Raman excitation
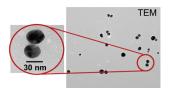
Figure 2. TEM image taken of fresh dimer solution. Particles have an average diameter of 30 nm. (a) A mixture of dimers and single spheres. (b) A dimer and a cluster of 4. (c) A cluster of 7. (d) A close-up of a single dimer.

volume is then estimated to be 0.137 pL. Given a concentration of 14.3 pM, there are approximately 1.1 dumbbells in the focal volume at any given time.

Raman measurements were performed by allowing the nanoparticles to freely diffuse through the probing volume, in a manner similar to that employed in Raman correlation spectroscopy.[41] Spectra are captured at signal integration times of 200 ms. After accumulation, spectra are sorted based on relative peak intensities and positions, and each category is subsequently averaged. Given that, on average, only 1.1 DSB molecules are present in the probing volume at any given time, the spectral signatures observed originate from molecules at concentrations in the single-molecule range. The advantage of this solution-based approach is that averaged spectra can be obtained from many copies of the molecules while still operating in the single-molecule regime.

Calculations. Electronic structure calculations were performed as an aid for the assignment of the observed spectra, which show significant variations. In these calculations, the silver nanospheres are represented by single atoms. The intent is to account in part for spectral changes associated with the chemical bonding and to distinguish such effects from plasmonic contributions. Calculations were performed using the B3LYP density functional in conjunction with double and triple-ζ quality basis sets. The 6-31g* and 6-311g** Pople-type basis sets were used to describe H, C, and S, whereas the def2-SVP and def2-TZVP basis sets were employed to describe the Ag atoms.[42] A systematic increase in basis set description reveals the expected trend in going from double ζ to triple ζ to experiment. The IR and Raman spectra were computed for the fully optimized global minima (all trans-anti) of DSB and DTDSB, as well as the silver-substituted monomers and dimers. We truncate the multielectron problem by approximating the silver nanoballs with silver atoms, as the simulation of the clusters is not computationally feasible. General agreement between the calculated and experimental spectra suggests that this approximation is reasonable for the purpose of (i) assigning the experimental vibrational spectra and (ii) distinguishing between the different chemical species probed in our experiments. All calculations were performed using the methodologies implemented in Gaussian 03.[43]

■ RESULTS

Dimer Formation. TEM images taken of the DSB-Ag sample show that the nanosphere dimers were successfully synthesized with a narrow size distribution. The average particle size is 30 nm. We find three categories of SERS active systems in our samples: (1) Ag nanosphere monomers, (2) Ag nanosphere dimers, and (3) clusters of three or more nanospheres. As seen in Figure 2, the majority of the solution is composed of monomers and dimers (~50%), while the fraction of clusters is much lower
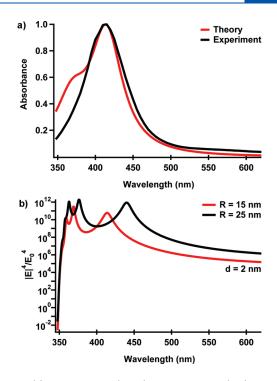

Figure 3. (a) Experimental (black) and calculated (red) extinction spectra. The calculation matches the experiment assuming 15 nm silver spheres with a 2 nm interparticle gap. (b) The calculated Raman enhancement factor due to the local field (E^4/E_0^4) as a function of excitation wavelength. The calculation predicts an enhancement of 6.1×10^5 at $\lambda = 532$ nm.

(~1%). DSB molecules are expected to be associated with each of these particle systems. Dimer particles contain at least one DSB molecule that acts as a linker. In addition, DSB molecules may cover the surface of the particles. Clusters are held together by multiple copies of the DSB linker, forming multiple hot spots in individual clusters.

Plasmonic Response. The ensemble absorption spectrum of the dimer preparation in aqueous solution is shown in Figure 3a. The spectrum exhibits a clear plasmon resonance that peaks at 415 nm. To extract estimates for the plasmonic enhancement from the spectrum, we have performed calculations using an analytical model for the plasmonic absorption of the dimer system. Our analytical model is based on describing the silver nanosphere dimer in bispherical coordinates, which allows exact electric field calculations for simple plasmonic systems with bispherical symmetry. More details on the computational method are documented in ref 44.

The calculated spectrum in Figure 3a, assuming a radius $R = 15$ nm for each of the silver nanospheres in the dimer and a nanogap of 2 nm, correctly reproduces the spectral maximum of the plasmon resonance. In addition, the calculation predicts a shoulder on the blue side of the spectrum which is not observed in the experiment. Although the sample contains a high percentage of silver nanosphere dimers, the presence of nanosphere monomers and clusters significantly perturbs the spectrum. The heterogeneity of the sample provides a reasonable explanation for the discrepancy between the experiments and calculations.

The calculated spectral dependence of the electric field enhancement is shown in Figure 3b. Two results are compared: two spheres with radii 15 nm and two spheres with radii 25 nm. In
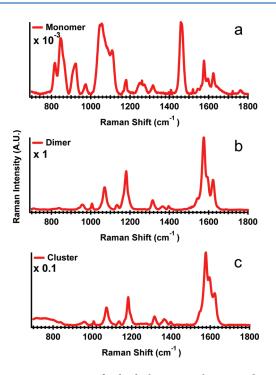
Figure 4. Raman spectra of individual nanoparticles assigned to number of spheres linked by DSB. (a) One sphere, (b) two spheres, and (c) three or more spheres. The presented spectra are averaged over six acquisitions, with 10 s of CCD exposure time per acquisition.

both cases, the separation d (surface to surface) is 2 nm. The highest field enhancements are observed close to the peak of the plasmon resonance, and substantial field enhancements also manifested at longer wavelengths. It should be noted that for larger particles the maximum field enhancement shifts to longer wavelengths. Hence, when exciting the dimer solutions into the red wing of the absorption band, larger particles are expected to contribute more than smaller particles to the overall process. In our experiments, the dimers are excited off resonance at 532 nm, where the enhancement of the field intensity is as high as 780. This results in a predicted plasmonic enhancement of 6.1×10^5.

Surface-Enhanced Raman Scattering. On the basis of the different ways in which the DSB molecule is associated with the nanosphere, we expect different SERS signatures for each of the three types of particle systems. On the basis of hydrodynamic (Stokes–Einstein) diffusion calculations, the average residence time of a silver nanostructure in the probing volume is 20 ms or longer, with longer residence times predicted for the larger clusters. At the signal acquisition rate of 200 ms, fluctuations of the spectral signals that can be associated with diffusion of particles in and out of the probing volume are observed. The different types of observed spectra are summarized in Figure 4. We assign the most frequently occurring spectrum to the nanosphere dimer (Figure 4b). The much weaker ($\sim10^3$ times) recurring spectrum of Figure 4a is attributed to nanosphere monomers. A third class of spectra, characterized by a much lower incidence rate and by much higher spectral intensities, is assigned to the clusters (Figure 4c). Occasionally, this class of strong spectra is observed continuously over several seconds, indicative of optical trapping.[45] The observation of trapping of larger particles provides further support for the assignment of the strongly enhanced spectra to clusters. The intensity differences between these distinct types of spectra ensure that only the
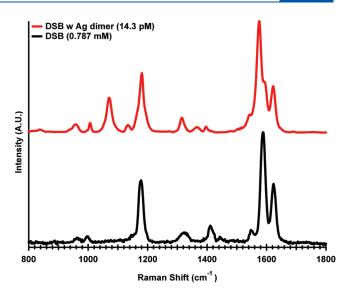

Figure 5. Surface-enhanced raman spectra of distyrylbenzene tethered between two silver nanospheres (top) compared to bare distyrylbenzene (bottom).
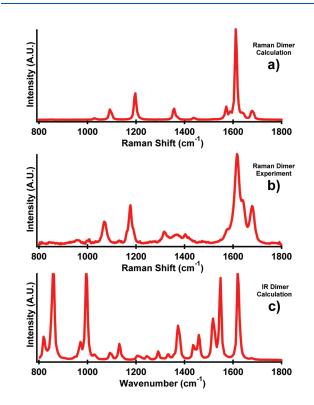

Figure 6. Comparison of distyrylbenzene dimer spectra: (a) calculated Raman dimer, (b) surface enhanced Raman spectra of the distyrylbenzene dimer, and (c) calculated IR dimer. The calculated spectra are for DSB terminated by a silver atom on each end, instead of the nanospheres.

particle type with the highest incidence rate in the focus will prevail in the averaged spectra during relatively short accumulation times.

To determine the Raman enhancement by nanosphere dimers, the Raman spectrum of bare DSB was also recorded. DSB was dissolved in dicloromethane (DCM) at a concentration of 0.787 mM. The solvent spectrum was then subtracted to obtain

Table 1. Experimental and Calculated Frequencies, Relative Intensities, and Spectral Assignments for the Dimer Spectrum

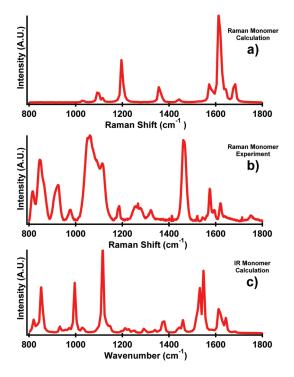| experiment dimer		theory				
Raman shift (cm^{-1})	relative intensity	Raman shift (cm^{-1})	Raman relative intensity	infrared shift (cm^{-1})	IR relative intensity	spectral assignment
1004	0.05	999	0.02	999	0.9444	vinyl CH out-of-plane bending
1130	0.03	1095	0.1	1095	0.07	HC≡CH dihedral bending on outer rings
1177	0.43	1132	0.01	1131	0.02	HC=CH dihedral bending on outer rings
1316	0.13	1208	0.33	1208	0.05	delocalized Ch wag
1367	0.1	1371	0.03	1375	0.33	vinyl CH wag
1409	0.1	1439	0.02	1439	0.16	HC≡CH dihedral bending on outer rings
1576	0.16	1586	0.1	-	-	C≡C aromatic stretch central ring
1616	1	1612	1	1612	0.16	delocalized C≡C stretch
1620	0.3	-	-	1622	0.84	C≡C aromatic stretch on outer rings
1641	0.49	1640	0.08	1640	0.1	aromatic C≡C stretch
1679	0.42	1680	0.0	1680	0.03	vinyl C≡C stretch

Figure 7. Comparison of distyrylbenzene monomer spectra: (a) calculated Raman monomer, (b) surface-enhanced Raman spectra of distyrylbenzene monomer, and (c) calculated IR monomer. The calculations are for a single silver atom attachment.

the bare DSB spectrum shown in Figure 5. The Raman enhancement factor (EF) was calculated using the equation[46]

$$ \text{EF} = (N_{ref}/N_{SERS}) \cdot (I_{SERS}/I_{ref}) \qquad (1) $$

where I_{SERS} and I_{ref} are the SERS intensity of the DSB attached to Ag particles and the normal Raman scattering intensity of a 0.787 mM DSB solution, respectively. Assuming a single DSB molecule per dimer, N_{SERS} and N_{ref} are the number of DSB molecules in the probing volume for the case of dimers and pure DSB, respectively. On the basis of this analysis for the prominent peaks near 1180 and 1590 cm^{-1}, we find a SERS enhancement of 3×10^6.

The 5-fold discrepancy between the observed enhancement and the prediction determined by the plasmonically enhanced local field can be entirely rationalized by the chemical contribution. For the considered vibrational modes, the calculated intensities show a factor of 2.3 increase upon attachment of one silver atom to DSB and a factor of 7.5 upon attachment of a silver atom at each end. This can be regarded as a lower limit to the chemical enhancement expected by binding to the more polarizable silver nanospheres and does not take into account preresonances with charge transfer states that can dominate Raman cross sections.[47] Nevertheless, based on the lower limit of the expected chemical contribution, the observed enhancement is in excellent agreement with the computed product of chemical and plasmonic enhancement factors, EF = 4.5 × 10^6.

Spectral Analysis. The Raman spectrum assigned to the single dimer (Figure 4b) is very similar to that of the bulk sample, which contains ∼50% dimers (Figure 5). The parentage of these spectra is clear by the comparison made with bare DSB in Figure 5. The calculated Raman spectrum of the dimer (Figure 6) appears to account for most of the experimental peaks, aside from features at 1130 and 1316 cm^{-1} (see Table 1). To understand the origin of these vibrations, we also simulated the IR spectrum of the molecule (see Figure 6c). The additional lines seen in the Raman spectrum can be assigned to IR active vibrations; however, there would have to be a special consideration as to why these particular lines appear in the spectrum. On the other hand, the SERS spectrum of the monomer cannot be solely assigned based on the computed Raman spectrum of the molecule (Figure 7). Only a few of the theoretical Raman peaks seem to appear in the experimental spectrum. Here, the combined experimental and computational results suggest that both the IR and Raman modes appear in the experiment (see Table 2). In repeated acquisitions of what appear as monomer spectra, we observe significant variations as illustrated by the three examples in Figure 8. Clearly, the tethered Ag nanoparticles play an important role in selecting which normal modes are enhanced and thus experimentally observed; moreover, variations in the spectrum of a given structure suggest that the orientation of the freely diffusing molecules in the local applied field control the observable spectrum. Thus, we next discuss the nature of the normal modes and their spectral variations.

Table 2. Experimental and Calculated Frequencies, Relative Intensities, and Spectral Assignments for the Monomer Spectrum[a]

experiment monomer		theory				
Raman shift (cm^{-1})	relative intensity	Raman shift (cm^{-1})	Raman relative intensity	infrared shift (cm^{-1})	IR relative intensity	spectral assignment
820	0.31	-	-	819	0.16	delocalized out-of-plane CH bending
854	0.62	-	-	854	0.53	aromatic out-of-plane CH bending
924	0.44	-	-	931	0.07	CSH bending β S
973	0.2	-	-	971	0.06	aromatic CH out-of-plane bending on α ring
1045	0.3	1096	0.11	1096	0.08	α C−S stretch
1111	0.5	1118	0.05	1116	1	β C−S stretch
1185	0.17	1200	0.49	1212	0.06	aromatic HC=CH dihedral bend on β ring
1461	1	-	-	1459	0.15	aromatic HC=CH dihedral bend on central ring
1598	0.3	1583	0.15	1581	0.04	delocalized aromatic C=C stretch
1623	0.23	1615	1	1614	0.27	delocalized aromatic C=C stretch mostly α ring

[a] The α ring refers to the aromatic ring closest to the metal nanoparticle, while the β ring refers to that farthest from the metal nanoparticle.
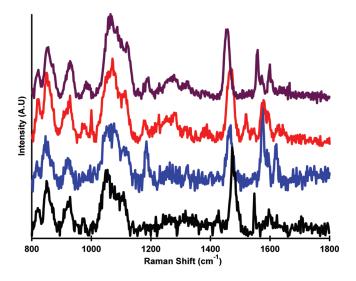

Figure 8. Comparison of four distinct distyrylbenzene monomer spectra.

A closer inspection of the spectra is instructive. The pure DSB spectrum shows several strong peaks, including signature aromatic C−H vibrations at 1175 cm^{-1} and the aromatic C=C stretching vibrations at 1600 cm^{-1}. The aromatic C=C vibrational range features three distinct peaks, with the strongest centered at 1588 cm^{-1}. Once the Ag particles are attached, however, this peak is shifted to 1574 cm^{-1}, and a shoulder at 1594 cm^{-1} becomes noticeable. Another important contrast between the spectra is the red shift of the in-plane aromatic C−H stretching vibrations in the 1300−1500 cm^{-1} range (see Table 1). The red shift of these peaks is attributed to the addition of the heavy Ag substituents. Another prominent peak which appears in the dimer spectrum at 1072 cm^{-1} is the C−S stretch, which is absent in the bare DSB spectrum.

Clear differences are noticeable when comparing the dimer and monomer SERS spectra. For instance, in the monomer spectrum the enhancement of the 1600 cm^{-1} modes is less than what is observed in the dimer, and remarkably, the lower frequency vibrations (800−1100 cm^{-1}), which are not Raman active, begin to appear. The largest peaks in the monomer spectrum belong to the C−S stretch (1044, 1111 cm^{-1}) and

the H−C=C−H dihedral bend coupled to the aromatic C=C stretching vibration of the ring adjacent to the Ag nanosphere (1461 cm^{-1}). When only one Ag ball is attached to the thiolated DSB, there are two different types of C−S vibrations: (1) C−S−Ag and (2) C−S−H, which explain the splitting of the C−S vibrations into two peaks at 1044 and 1111 cm^{-1}. Moreover, the free C−S−H moiety is capable of H-bonding with neighboring water molecules, a consideration that may explain the observed broadening of the bands associated with the C−S stretch.

■ DISCUSSION

The silver nanosphere dimers prepared in this study offer several attractive features relative to previous dimer preparations. First, the yield of dimers is high. We have consistently prepared samples in which more than 50% of the resulting particles are dimers. Second, the dimers inherently incorporate the DSB molecule. Because the DSB molecules are connected exclusively through thiol linkers to the nanospheres, the positioning and orientation of the target molecule are well-defined. This implies that the majority of DSB in the preparation is positioned directly in the nanogap hot spot. Finally, the high yield of dimer formation enables direct measurements in solution. This approach offers good averaging statistics while maintaining low-concentration conditions in the single-molecule regime.

The three distinct types of SERS spectra that we observe in our solution-based assay indicate that three major particle systems contribute to the time-integrated SERS spectrum. From TEM experiments, we clearly observe three categories of particle units. The relative incidence rates and spectral intensities of the monomer, dimer, and cluster systems in the Raman measurements are all in accordance with the relative concentration of each of these particle systems. In fresh samples, the dimer spectra predominate. We have observed, however, that the incidence rate of the dimer Raman component reduces as the samples age (shelf time of one month or more), which is accompanied first by an increase of the incidence rate of the cluster spectra. As the sample continues to age (more than several months), the monomer spectrum begins to dominate. Subsequent TEM studies confirm that as the samples age the monomer concentration grows at the expense of dimers and clusters (see Figure 1). These consistent

15905

dx.doi.org/10.1021/jp205055h |*J. Phys. Chem. C* 2011, 115, 15900–15907

observations give further confidence to the assignment of the monomer, dimer, and cluster spectra.

The most remarkable observation is the appearance of non-Raman active modes in the spectra of DSB attached to a single nanosphere. The new peaks can be assigned to the IR active modes. Of particular notice are the lower-frequency shifts at 820 and 850 cm^{-1}, which are out-of-plane C–H bending modes. Also, a relatively strong response is seen for C–S–H bending at 930 cm^{-1}, which can only occur in a monomer structure.

The observed enhanced IR active modes clearly indicate that the incorporation of the nanoantennae changes the selection rules for Raman scattering. The Ag nanoballs render the observation of other (non-Raman active) internal modes of the molecule possible. This has been previously observed in experiments[48−51] and rationalized by Ayar et al. in terms of the gradient-field Raman (GFR) effect.[35] Through Taylor series expansion of the induced polarization, they have argued that besides the standard Raman active modes given by $d\alpha_{a,b}/dq \neq 0$ in a constant electric field E_b the presence of a field gradient on the length scale of the molecule leads to Raman scattering from polarizable modes, with cross sections determined by $\alpha_{a,b} \cdot dE_b/dq$. Here $\alpha_{a,b}$ with $a,b = x,y,z$ are elements of the molecular polarizability tensor. This electric field gradient effect changes the Raman selection rules.[35,48−51] The tensor nature of the polarizability clarifies that there will be fluctuations associated with the orientation of the molecule relative to the local field gradient. These are most evident in the fluctuations seen in the spectra of Figure 8. For example, the in-plane H–C≡C–H dihedral bend on the ring adjacent to the nanosphere, which is the most prominent in this spectrum, displays relative intensity changes. Given its proximity to the antenna, and the general behavior of the electric field gradient in this region, this moiety is expected to be sensitive to the orientation of the molecule in the field. Indeed, fluctuations are manifested in the in-plane (1519 cm^{-1}, 1185 cm^{-1}) and out-of-plane (973 cm^{-1}) aromatic H–C≡C–H dihedral bends on this ring.

Clearly, the sensitivity of our measurements is high enough to discern the contribution of DSB molecules associated with monomer silver nanospheres. Monomer nanosphere systems are typically considered ineffective in producing detectable signals from tethered single molecules.[29,52] We attribute this high level of sensitivity observed here to the optimized conditions of the solution-based assay.

CONCLUSIONS

Silver nanospheres were synthesized successfully, with a narrow size dispersion, and were attached to dithiolated DSB molecules to create SERS active nanostructures. The final solution consisted of ∼50% DSB-linked Ag nanosphere dimers, a small fraction of clusters containing three or more Ag spheres, and the rest were single Ag spheres. The measured extinction spectra of the ensemble could be reproduced theoretically, assuming 15 nm spheres separated by a 2 nm gap, consistent with the length of the linker. The SERS spectra of individual particles could be recorded in aqueous solution and assigned to monomer, dimer, and clusters of nanospheres. The Raman spectra of the dimers closely resemble those of bare DSB. Assuming that dimers are attached by a single DSB linker, an experimental Raman enhancement factor of $EF_{exp} = 3 \times 10^6$ is measured. This value is slightly smaller than the theoretical estimate, $EF = (EF_p)(EF_c) = 4.5 \times 10^6$, which is obtained as

the product of physical and chemical factors. The calculated physical enhancement factor due to the enhanced local field at the intersphere junction is $EF_p = 6.1 \times 10^5$; the estimated chemical enhancement factor $EF_c = 7.5$ is based on DFT calculations of DSB attached to a silver atom on each end. The enhancement factors, the geometry of dimers based on TEM, and extinction spectra provide consistent evidence that the observed dimer spectra are those of single molecules. Indeed, based on the synthesis, additional molecules can be attached to the surface of Ag spheres, as verified by the observation SERS spectra of DSB on monomeric nanospheres. However, the SERS spectra of single spheres are 2−3 orders of magnitude weaker than that of the dimer, which establishes that only bridging molecules contribute to the dimer spectrum. While we do not definitively establish that there is only one bridging molecule per dimer, given the dynamic range of detection, the present work validates the concept of equipping molecules with nanoantennae to address them individually and to interrogate them under ambient conditions.

AUTHOR INFORMATION

Corresponding Author

*E-mail: aapkaria@uci.edu.

REFERENCES

(1) Fleischmann, M.; Hendra, P. J.; McQuillan, A. J. *Chem. Phys. Lett.* **1974**, *26*, 163.

(2) Jeanmaire, D. L.; Van Duyne, R. P. *J. Electroanal. Chem.* **1977**, *84*, 1.

(3) Moskovits, M. *J. Chem. Phys.* **1978**, *69*, 4159.

(4) Otto, A. *Surf. Sci.* **1978**, *75*, L392.

(5) Brockman, J. M.; Nelson, B. P.; Corn, R. M. *Annu. Rev. Phys. Chem.* **2000**, *51*, 41.

(6) Haes, A. J.; Van Duyne, R. P. *J. Am. Chem. Soc.* **2002**, *124*, 10596.

(7) Nowak-Lovato, K. L.; Rector, K. D. *Appl. Spectrosc.* **2009**, *63*, 387.

(8) Kneipp, K.; Wang, Y.; Kneipp, H.; Itzkan, I.; Dasari, R. R.; Feld, M. S. *Phys. Rev. Lett.* **1996**, *76*, 2444.

(9) Nie, S.; Emory, S. R. *Science* **1997**, *275*, 1102.

(10) Xu, H.; Kall, M. *Phys. Rev. Lett.* **2002**, *89*, 246802.

(11) Sawai, Y.; Takimoto, B.; Nabika, H.; Ajito, K.; Murakoshi, K. *J. Am. Chem. Soc.* **2007**, *129*, 1658.

(12) Dieringer, J. A.; Lettan, R. B.; Scheidt, K. A.; Van Duyne, R. P. *J. Am. Chem. Soc.* **2007**, *129*, 16249.

(13) Vlckovấ, B.; Moskovits, M.; Pavel, I.; Siskovấ, K.; Slấdkovấ, M.; Slouf, M. *Chem. Phys. Lett.* **2008**, *455*, 131.

(14) Pettinger, B.; Wenning, U. *Chem. Phys. Lett.* **1978**, *56*, 253.

(15) Wood, T. H.; Klein, M. V.; Zwemer, D. A. *Surf. Sci.* **1981**, *107*, 625.

(16) Seki, H. *J. Vac. Sci. Technol.* **1981**, *18*, 633.

(17) Creighton, J. *Surf. Sci.* **1983**, *124*, 209.

(18) Moody, R. L.; Vo-Dinh, T.; Fletcher, W. H. *Appl. Spectrosc.* **1987**, *41*, 966.

(19) Kottmann, J.; Martin, O. *Opt. Express* **2001**, *8*, 655.

15906

dx.doi.org/10.1021/jp205055h |*J. Phys. Chem. C* 2011, 115, 15900–15907

(20) Jeong, D. H.; Zhang, Y. X.; Moskovits, M. *J. Phys. Chem. B* **2004**, *108*, 12724.

(21) Srituravanich, W.; Fang, N.; Sun, C.; Luo, Q.; Zhang, X. *Nano Lett.* **2004**, *4*, 1085.

(22) Dieringer, J. A.; McFarland, A. D.; Shah, N. C.; Stuart, D. A.; Whitney, A. V.; Yonzon, C. R.; Young, M. A.; Zhang, X.; Van Duyne, R. P. *Faraday Discuss.* **2006**, *132*, 9.

(23) Aravind, P.; Nitzan, A.; Metiu, H. *Surf. Sci.* **1981**, *110*, 189.

(24) Hao, E.; Schatz, G. C. *J. Chem. Phys.* **2004**, *120*, 357.

(25) Chu, P.; Mills, D. L. *Phys. Rev. Lett.* **2007**, *99*, 127401.

(26) Letnes, P. A.; Simonsen, I.; Mills, D. L. *Phys. Rev. B* **2011**, *83*, 075426.

(27) Su, X.; Zhang, J.; Sun, L.; Koo, T.; Chan, S.; Sundararajan, N.; Yamakawa, M.; Berlin, A. A. *Nano Lett.* **2005**, *5*, 49.

(28) Braun, G.; Pavel, I.; Morrill, A. R.; Seferos, D. S.; Bazan, G. C.; Reich, N. O.; Moskovits, M. *J. Am. Chem. Soc.* **2007**, *129*, 7760.

(29) Camden, J. P.; Dieringer, J. A.; Wang, Y.; Masiello, D. J.; Marks, L. D.; Schatz, G. C.; Van Duyne, R. P. *J. Am. Chem. Soc.* **2008**, *130*, 12616.

(30) Braun, G. B.; Lee, S. J.; Laurence, T.; Fera, N.; Fabris, L.; Bazan, G. C.; Moskovits, M.; Reich, N. O. *J. Phys. Chem. C* **2009**, *113*, 13622.

(31) Kleinman, S. L.; Ringe, E.; Valley, N.; Wustholz, K. L.; Phillips, E.; Scheidt, K. A.; Schatz, G. C.; Van Duyne, R. P. *J. Am. Chem. Soc.* **2011**, *133*, 4115.

(32) Li, W.; Camargo, P. H.; Lu, X.; Xia, Y. *Nano Lett.* **2009**, *9*, 485.

(33) Daniel, M.; Astruc, D. *Chem. Rev.* **2004**, *104*, 293.

(34) Seferos, D. S.; Banach, D. A.; Alcantar, N. A.; Israelachvili, J. N.; Bazan, G. C. *J. Org. Chem.* **2004**, *69*, 1110.

(35) Ayars, E. J.; Hallen, H. D.; Jahncke, C. L. *Phys. Rev. Lett.* **2000**, *85*, 4180.

(36) Turkevich, J.; Stevenson, P. C.; Hillier, J. *Discuss. Faraday Soc.* **1951**, *11*, 55.

(37) Lee, P. C.; Meisel, D. *J. Phys. Chem.* **1982**, *86*, 3391.

(38) Loweth, C. J.; Caldwell, W. B.; Peng, X.; Alivisatos, A. P.; Schultz, P. G. *Angew. Chem., Int. Ed.* **1999**, *38*, 1808.

(39) Jenkins, F. A.; White, H. E. *Fundamentals of Optics*, 4th ed.; Mcgraw-Hill College: New York, 1976.

(40) Zimmerley, M.; Anthony McClure, R.; Choi, B.; Potma, E. *Appl. Opt.* **2009**, *48*, D79.

(41) Schrof, W.; Klingler, J. F.; Rozouvan, S.; Horn, D. *Phys. Rev. E* **1998**, *57*, R2523.

(42) Peterson, K. A.; Figgen, D.; Goll, E.; Stoll, H.; Dolg, M. *J. Chem. Phys.* **2003**, *119*, 11113.

(43) Frisch, M. J. et al. *Gaussian 03*, revision C.02; Gaussian, Inc.: Wallingford, CT, 2004.

(44) Chu, P.; Mills, D. L. *Phys. Rev. B: Condens. Matter Mater. Phys.* **2008**, *77*, 045416.

(45) Juan, M. L.; Righini, M.; Quidant, R. *Nat. Photon* **2011**, *5*, 349–356.

(46) Luo, W.; van der Veer, W.; Chu, P.; Mills, D. L.; Penner, R. M.; Hemminger, J. C. *J. Phys. Chem. C* **2008**, *112*, 11609.

(47) Branigan, E. T.; Halberstadt, N.; Apkarian, V. A. *J. Chem. Phys.* **2011**, *134*, 174503.

(48) Hermann, P.; Hermelink, A.; Lausch, V.; Holland, G.; Möller, L.; Bannert, N.; Naumann, D. *Analyst* **2011**, *136*, 1148.

(49) Berweger, S.; Raschke, M. B. *J. Raman Spectrosc.* **2009**, *40*, 1413.

(50) Neacsu, C. C.; Dreyer, J.; Behr, N.; Raschke, M. B. *Phys. Rev. B* **2006**, *73*, 193406.

(51) Lu, H. P. *J. Phys.: Condens. Matter* **2005**, *17*, R333–R355.

(52) Moskovits, M. *J. Raman Spectrosc.* **2005**, *36*, 485.

15907

dx.doi.org/10.1021/jp205055h |*J. Phys. Chem. C* 2011, 115, 15900–15907